Soft-gluon resummation for squark and gluino hadroproduction

Wim Beenakker

Theoretical High Energy Physics, Radboud University Nijmegen, P.O. Box 9010
NL-6500 GL Nijmegen, The Netherlands

Silja Brensing, Michael Krämer, Anna Kulesza

Institut für Theoretische Physik, RWTH Aachen University
D-52056 Aachen, Germany

Eric Laenen

ITFA, University of Amsterdam, Valckenierstraat 65, 1018 XE Amsterdam,
ITF, Utrecht University, Leuvenlaan 4, 3584 CE Utrecht
Nikhef Theory Group, Science Park 105, 1098 XG Amsterdam, The Netherlands

Irene Niessen

Theoretical High Energy Physics, Radboud University Nijmegen, P.O. Box 9010
NL-6500 GL Nijmegen, The Netherlands

ABSTRACT: We consider the resummation of soft gluon emission for squark and gluino hadroproduction at next-to-leading-logarithmic (NLL) accuracy in the framework of the minimal supersymmetric standard model. We present analytical results for squark-squark and squark-gluino production and provide numerical predictions for all squark and gluino pair-production processes at the Tevatron and at the LHC. The size of the soft-gluon corrections and the reduction in the scale uncertainty are most significant for processes involving gluino production. At the LHC, where the sensitivity to squark and gluino masses ranges up to 3 TeV, the corrections due to NLL resummation over and above the NLO predictions can be as high as 35% in the case of gluino-pair production, whereas at the Tevatron, the NLL corrections are close to 40% for squark-gluino final states with sparticle masses around 500 GeV.

arXiv:0909.4418v1 [hep-ph] 24 Sep 2009

Contents

1. Introduction

The search for supersymmetry (SUSY) [1, 2] is among the most important tasks at current and future colliders. Squarks and gluinos, the coloured supersymmetric particles, are expected to be produced most copiously in hadronic collisions. Searches at the proton–antiproton collider Tevatron with a centre-of-mass energy of $\sqrt{S} = 1.96$ TeV have placed lower limits on squark and gluino masses in the range of 300-400 GeV [3, 4]. The proton–proton collider LHC with $\sqrt{S} = 14$ TeV design energy will extend the range of sensitivity to squarks and gluinos with masses up to about 3 TeV [5, 6, 7].

In the minimal supersymmetric extension of the Standard Model (MSSM) [8, 9] with R-parity conservation, squarks and gluinos are pair-produced in collisions of two hadrons h_1 and h_2:

$$h_1 h_2 \rightarrow \tilde{q}\tilde{q}, \tilde{q}\bar{\tilde{q}}, \tilde{q}\tilde{g}, \tilde{g}\tilde{g} + X. \tag{1.1}$$

In Eq. (1.1) and throughout the rest of this paper we suppress the chiralities of the squarks $\tilde{q} = (\tilde{q}_L, \tilde{q}_R)$ and do not explicitly state the charge-conjugated processes. We include squarks $\tilde{q}$ of any flavour except for top squarks. The production of top squarks [10] has to be considered separately since the strong Yukawa coupling between top quarks, top squarks and Higgs fields gives rise to potentially large mixing effects and mass splitting [11].

Accurate theoretical predictions for inclusive cross sections are crucial to derive exclusion limits for squark and gluino masses [3, 4] and, in the case of discovery, can be used to determine sparticle masses [12] and properties [13]. The cross sections for the squark and gluino pair-production processes (1.1) are known at next-to-leading order (NLO) in SUSY-QCD [14, 15, 16]. Electroweak corrections to the $\mathcal{O}(\alpha_s^2)$ tree-level production [17, 18, 19, 20] and the electroweak Born production channels of $\mathcal{O}(\alpha\alpha_s)$ and $\mathcal{O}(\alpha^2)$ [21, 22] are significant for the pair production of SU(2)-doublet squarks $\tilde{q}_L$ and at large invariant masses in general, but they are moderate for total cross sections summed over all squark species.

The NLO SUSY-QCD corrections to squark and gluino hadroproduction reduce the renormalization- and factorization-scale dependence of the predictions. In general these corrections also significantly increase the cross section with respect to the Born predictions [23, 24, 25] if the renormalization and factorization scales are chosen close to the average mass of the pair-produced sparticles. A significant part of these large corrections can be attributed to the threshold region where the partonic centre-of-mass energy is close to the kinematic threshold for producing massive particles. In this region the NLO corrections are dominated by the contributions due to soft gluon emission off the coloured particles in the initial and final state and by the Coulomb corrections due to the exchange of gluons between the massive sparticles in the final state. The soft-gluon corrections can be taken into account to all orders in perturbation theory by means of threshold resummation.

Previous work has addressed the soft-gluon resummation for squark-antisquark and gluino-gluino production at next-to-leading-logarithmic (NLL) accuracy [26, 27]. For the squark-antisquark production process the dominant contribution to the next-to-next-to-leading order (NNLO) correction coming from the resummed cross section at next-to-next-to-leading-logarithmic (NNLL) level has been studied in [28]. Moreover, a formalism allowing for the resummation of soft and Coulomb gluons in the production of coloured sparticles has been presented in [29, 30], and bound state effects have been studied for gluino-pair production in Ref. [31]. Additionally, threshold resummation for single colour-octet scalar production at the LHC has been investigated in [32].

In this work, we present the analytical components needed to perform NLL resummation for squark-squark and squark-gluino pair-production. In addition, we provide numerical predictions for the entire set (1.1) of pair-production processes of coloured sparticles at the Tevatron and the LHC.

The paper is structured as follows. In section 2 we review the formalism of soft-gluon

resummation. The calculation of the one-loop soft anomalous dimension matrices for the $\tilde{q}\tilde{q}$ and $\tilde{q}\tilde{g}$ production processes is discussed in section 3. We present numerical results for squark and gluino production at the Tevatron and the LHC in section 4 and conclude in section 5. A more detailed description of certain aspects of our calculation and some explicit formulae that enter the expressions for the resummed cross sections are collected in the appendices.

2. Soft-gluon resummation

In this section we review the formalism of threshold resummation for the production of a pair of coloured massive particles. Since the corresponding theoretical expressions have already been discussed in detail in Ref. [27], we shall be brief.

The inclusive hadroproduction cross section $\sigma_{h_1 h_2 \to kl}$ for two massive SUSY particles k and l, where k, l can be a squark ($\tilde{q}$), antisquark ($\bar{\tilde{q}}$) or gluino ($\tilde{g}$), can be written in terms of its partonic version $\sigma_{ij \to kl}$ as

$$
\sigma_{h_1 h_2 \to kl}\big(\rho, \{m^2\}\big) = \sum_{i,j} \int dx_1 dx_2\, d\hat{\rho}\, \delta\left(\hat{\rho} - \frac{\rho}{x_1 x_2}\right)
$$
$$
\times\, f_{i/h_1}(x_1, \mu^2)\, f_{j/h_2}(x_2, \mu^2)\, \sigma_{ij \to kl}\big(\hat{\rho}, \{m^2\}, \mu^2\big), \quad (2.1)
$$

where $\{m^2\}$ denotes all masses entering the calculations, i, j are the initial parton flavours, f_{i/h_1} and f_{j/h_2} the parton distribution functions, and μ is the common factorization and renormalization scale. The hadronic threshold for inclusive production of two final-state particles with masses m_3 and m_4 corresponds to a hadronic center-of-mass energy squared that is equal to $S = (m_3 + m_4)^2$. Thus we define the threshold variable ρ, measuring the distance from threshold in terms of energy fraction, as

$$
\rho = \frac{(m_3 + m_4)^2}{S}.
$$

The partonic equivalent of this threshold variable is defined as $\hat{\rho} = \rho/(x_1 x_2)$, where $x_{1,2}$ are the momentum fractions of the partons. This is a generalized version of the threshold variable used e.g. in Ref. [27]. It accounts for unequal masses of the pair-produced particles in the final state, making it applicable to the case of squark-gluino production.

In the threshold region, the most dominant contributions to the higher-order QCD corrections due to soft gluon emission have the general form[1]

$$
\alpha_s^n \log^m \beta^2 \ , \quad m \leq 2n \qquad \text{with} \qquad \beta^2 \equiv 1 - \hat{\rho} = 1 - \frac{(m_3 + m_4)^2}{s}, \qquad (2.2)
$$

where $s = x_1 x_2 S$ is the partonic center-of-mass energy squared. The resummation of the soft-gluon contributions is performed after taking a Mellin transform (indicated by a tilde)

---

[1]See section 3 for more discussion on the form of a threshold variable in the case of unequal masses.

of the cross section,

$$\tilde{\sigma}_{h_1 h_2 \to kl}(N, \{m^2\}) \equiv \int_0^1 d\rho \, \rho^{N-1} \, \sigma_{h_1 h_2 \to kl}(\rho, \{m^2\}) \tag{2.3}$$

$$= \sum_{i,j} \tilde{f}_{i/h_1}(N+1, \mu^2) \, \tilde{f}_{j/h_2}(N+1, \mu^2) \, \tilde{\sigma}_{ij \to kl}(N, \{m^2\}, \mu^2) \, .$$

The logarithmically enhanced terms are then of the form $\alpha_s^n \log^m N$, $m \leq 2n$, with the threshold limit $\beta \to 0$ corresponding to $N \to \infty$. The resummed cross section takes the schematic form [33, 34]

$$\tilde{\sigma}_{h_1 h_2 \to kl}(N) = \exp\left[L g_1(\alpha_s L) + g_2(\alpha_s L) + \ldots \right] \times P(\alpha_s), \tag{2.4}$$

in which all dependence on the large logarithm $L = \log N$ occurs in the exponent, and no term in the perturbative series $P(\alpha_s)$ grows with increasing N. Keeping only the g_1 term constitutes the leading logarithmic (LL) approximation, including also the g_2 term is called the next-to-leading logarithmic (NLL) approximation, etc. Up to NLL accuracy it suffices to keep the lowest-order term in P.

The all-order summation of such logarithmic terms depends on the near-threshold factorization of the cross sections into functions that each capture the effects of classes of radiation effects: hard, collinear (including soft-collinear), and wide-angle soft radiation [33, 34, 35, 36, 37, 38]

$$\tilde{\sigma}_{ij \to kl}(N, \{m^2\}, \mu^2) = \Delta_i(N+1, Q^2, \mu^2) \, \Delta_j(N+1, Q^2, \mu^2)$$

$$\times \sum_{IJ} H_{ij \to kl, JI}(N, \{m^2\}, \mu^2) \, \bar{S}_{ij \to kl, IJ}(Q/(N\mu), \mu^2), \tag{2.5}$$

where we have introduced the hard scale $Q^2 = (m_3 + m_4)^2$. Before we comment on each function separately, we recall that soft radiation is coherently sensitive to the colour structure of the hard process from which it is emitted [39, 35, 40, 36]. The various structures are labelled by the indices I, J in a way made more precise further below.

The functions Δ_i and Δ_j sum the effects of the (soft-)collinear radiation from the incoming partons. They are process-independent and do not depend on the colour structures. They contain the leading logarithmic dependence, as well as part of the subleading logarithmic behaviour, and are listed e.g. in Ref. [27].

The function $H_{ij \to kl, JI}$ incorporates only higher-order effects of hard, off-shell partons and therefore does not contain $\log N$ dependence. This hard function depends on the colour representations of the external particles in the partonic process. There are usually multiple tensors c_I that can connect these colour representations, where I labels the possible tensors. For instance, in the case of squark-antiquark (with colour indices a_3, a_4) production by the annihilation of light quarks (with colour indices a_1, a_2) there are two colour tensors, which may be chosen as

$$c_1(a_1, a_2; a_3, a_4) = \delta_{a_1 a_2} \, \delta_{a_3 a_4} \qquad (s\text{–channel singlet}),$$

$$c_2(a_1, a_2; a_3, a_4) = T^c_{a_1 a_2} \, T^c_{a_3 a_4} \qquad (s\text{–channel octet}). \tag{2.6}$$

The hard function $H_{ij\to kl,JI}$ is a matrix in this colour-tensor space, with the indices JI indicating the colour structure. Note that we paired the indices in example (2.6) according to the s-channel. Other choices are possible as well [39, 40, 37], but choosing an s-channel basis will be convenient at threshold.

The soft function $\bar{S}_{ij\to kl,IJ}$ in Eq. (2.5) is also a matrix in colour-tensor space, since soft emissions mix the connecting colour tensors. This soft function is constructed [40, 37] from an eikonal cross section, which in turn is defined in terms of the square of expectation values of products of Wilson-line operators belonging to the external particles in the process. These Wilson lines generate to all orders the soft-gluon radiation in the process and depend on the direction and colour representation of the corresponding external particle. To avoid double counting with the Δ_i and Δ_j factors in Eq. (2.5), the expectation values are divided by the square of expectation values of the Wilson lines themselves. In this way, collinear-soft radiation already included in the Δ_i and Δ_j factors is removed. What remains is a soft function whose perturbation series takes the form $\alpha_{\rm s}^n \log^m N$, $m \leq n$, and therefore contributes only at NLL accuracy.

Although the combination of the soft and collinear functions in the cross section is gauge invariant, the functions themselves are not automatically separately gauge invariant. The collinear functions only depend on the colour representations of the incoming partons. Therefore the gauge dependence of the soft function cannot depend on the colour structure of the process either. This implies that we can make the soft and collinear functions separately gauge invariant by rescaling them with a scalar in colour-tensor space. This rescaling has implicitly been performed in Eq. (2.5), where the soft function has been divided by $\sqrt{S_{i\bar{i}}^{\rm sing}}\sqrt{S_{j\bar{j}}^{\rm sing}}$ as indicated by the bar on $\bar{S}_{ij\to kl,IJ}$. The factor $S_{i\bar{i}}^{\rm sing}$ is the soft function for two incoming Wilson lines of flavour i and $\bar{i}$ annihilating into a colour-singlet[2]. By taking the square root of such a soft function, we effectively isolate the gauge dependence of a single line. Therefore this procedure works not only for $q\bar{q}$ or gg initial states but also for initial states that cannot annihilate into a colour-singlet, such as qg and qq. To compensate for the division factor in the soft function, the collinear functions Δ_i and Δ_j have been multiplied by the factors $\sqrt{S_{i\bar{i}}^{\rm sing}}$ and $\sqrt{S_{j\bar{j}}^{\rm sing}}$ respectively. Analytical expressions for these functions given in the literature (see e.g. Ref. [27]) explicitly include this multiplicative factor.

Near threshold the soft function reduces considerably. For the inclusive cross section and our choice of colour basis, the matrix $\bar{S}_{ij\to kl,IJ}$ becomes diagonal in colour-tensor space in the threshold limit $\beta \to 0$ [27]. In this limit we have (suppressing particle flavour labels)

$$\lim_{\beta\to 0} \bar{S}_{IJ}\big(Q/(N\mu),\mu^2\big) = \delta_{IJ}\, S_{IJ}^{(0)}\, \Delta_I^{\rm (s)}\big(Q/(N\mu),\mu^2\big) \tag{2.7}$$

with

$$\Delta_I^{\rm (s)}\big(Q/(N\mu),\mu^2\big) = \exp\Big[\int_\mu^{Q/N}\frac{dq}{q}\,\frac{\alpha_{\rm s}(q)}{\pi}\, D_I\Big], \tag{2.8}$$

---

[2]Note that if the colour representations are **3** and $\bar{\textbf{3}}$ this corresponds to the Drell-Yan process. For octets, it corresponds to Higgs production by gluon fusion.

where $S_{IJ}^{(0)}$ is the lowest-order expression for the soft function, given by

$$S_{IJ}^{(0)} = \mathrm{tr}\left(c_I^\dagger c_J\right).$$ (2.9)

The one-loop coefficients D_I are defined by

$$D_I \equiv \lim_{\beta \to 0} \frac{\pi}{\alpha_{\mathrm{s}}} 2\,\mathrm{Re}\left(\bar{\Gamma}_{II}\right).$$ (2.10)

The values of the D_I coefficients for $\tilde{q}\bar{\tilde{q}}$ and $\tilde{q}\tilde{g}$ production are calculated in section 3.4.3. The form of Eq. (2.8) follows from a renormalization-group equation for $\bar{S}_{IJ}(Q/(N\mu))$ [35, 37], with one-loop anomalous dimensions $\bar{\Gamma}_{ij\to kl,IJ}$, often referred to as the "soft" anomalous-dimension matrix. If the calculations are performed in the axial-gauge with gauge vector n^μ, the one-loop anomalous dimensions are given by

$$\bar{\Gamma}_{IJ} = \Gamma_{IJ} - \frac{\alpha_{\mathrm{s}}}{2\pi} \sum_{p=\{i,j\}} C_{2,p}\left(1 - \log\left(2\frac{(v_p \cdot n)^2}{|n|^2}\right) - i\pi\right)\delta_{IJ},$$ (2.11)

where the sum is over the two incoming particles, and $|n|^2 = -n^2 - i\epsilon$, see Ref. [39]. The dimensionless vector v_p is given by the momentum of the incoming massless particle p multiplied by $\sqrt{2/s}$. The factors $C_{2,p}$ are either C_F or C_A, depending on whether p is a quark or gluon, respectively. The subtraction exhibited in Eq. (2.11) results from the division by the factor $\sqrt{S_{i\bar{i}}^{\mathrm{sing}}}\sqrt{S_{j\bar{j}}^{\mathrm{sing}}}$ described before. The matrix Γ_{IJ} is the anomalous dimension matrix of the products of Wilson-line operators connected by the various possible colour tensors mentioned earlier. More details on its calculation are given in section 3.4.

In the threshold limit the resummed partonic cross section becomes

$$\tilde{\sigma}_{ij\to kl}^{(\mathrm{res})}\left(N, \{m^2\}, \mu^2\right) = \sum_I \tilde{\sigma}_{ij\to kl,I}^{(0)}\left(N, \{m^2\}, \mu^2\right) C_{ij\to kl,I}\left(N, \{m^2\}, \mu^2\right)$$ (2.12)

$$\times \Delta_i(N+1, Q^2, \mu^2)\,\Delta_j(N+1, Q^2, \mu^2)\,\Delta_{ij\to kl,I}^{(\mathrm{s})}\left(Q/(N\mu), \mu^2\right),$$

where $\tilde{\sigma}_{ij\to kl,I}^{(0)}$ are the leading-order (LO) cross sections in Mellin-moment space. For the case of $\tilde{q}\bar{\tilde{q}}$ and $\tilde{q}\tilde{g}$ production we present them in appendix A. The functions $C_{ij\to kl,I}$ are of perturbative nature and contain information about hard contributions beyond leading order. This information is only relevant beyond NLL accuracy and therefore we keep $C_{ij\to kl,I} = 1$ in our calculations.

Having constructed the NLL cross-section in the Mellin-moment space, the inverse Mellin transform has to be performed in order to recover the hadronic cross section $\sigma_{h_1 h_2 \to kl}$. In order to retain the information contained in the NLO cross sections [14, 15, 16], the NLO and NLL results are combined through a matching procedure that avoids double counting of the logarithmic terms in the following way:

$$\sigma_{h_1 h_2 \to kl}^{(\mathrm{NLL+NLO\ matched})}\left(\rho, \{m^2\}, \mu^2\right) = \sigma_{h_1 h_2 \to kl}^{(\mathrm{NLO})}\left(\rho, \{m^2\}, \mu^2\right)$$ (2.13)

$$+ \sum_{i,j=q,\bar{q},g} \int_{\mathrm{CT}} \rho^{-N}\,\tilde{f}_{i/h_1}(N+1, \mu^2)\,\tilde{f}_{j/h_2}(N+1, \mu^2)$$

$$\times \left[\tilde{\sigma}_{ij\to kl}^{(\mathrm{res})}\left(N, \{m^2\}, \mu^2\right) - \tilde{\sigma}_{ij\to kl}^{(\mathrm{res})}\left(N, \{m^2\}, \mu^2\right)|_{(\mathrm{NLO})}\right].$$

We adopt the "minimal prescription" of Ref. [41] for the contour CT of the inverse Mellin transform in Eq. (2.13). In order to use standard parametrizations of parton distribution functions in x-space we employ the method introduced in Ref. [42].

3. Soft anomalous dimensions and Born cross sections for $\tilde{q}\tilde{q}$ and $\tilde{q}\tilde{g}$ production

3.1 Kinematics

To set the stage for the discussion of the soft anomalous dimensions we first introduce the relevant kinematical definitions that are used in the calculation. We consider the following generic process

$$i(a_1, p_1)\, j(a_2, p_2) \;\rightarrow\; k(a_3, p_3)\, l(a_4, p_4)\,, \tag{3.1}$$

where the colour indices a_i and the momenta of the particles p_i are given in parentheses. In those cases where a final-state squark features in the process, summation over both squark chiralities ($\tilde{q}_L$ and $\tilde{q}_R$) and all possible squark flavours is implied, the latter being restricted by the choice of initial-state quark flavours. For the processes investigated here, i.e. squark-squark ($kl = \tilde{q}\tilde{q}$) and squark-gluino ($kl = \tilde{q}\tilde{g}$) production, top-squark final states are not possible since top quarks are excluded as initial-state partons. In view of the absence of top-squark final states, all squark-flavour and chirality states are considered to be mass degenerate with mass $m_{\tilde{q}}$. The gluino mass is denoted by $m_{\tilde{g}}$.

All analytical results presented in section 3 are derived for a general SU(N_C)-theory, with N_C the number of colours. This means that the colour indices a_i for gluons and gluinos can take $N_C^2 - 1$ different values, since these particles are in the adjoint representation. For (s)quarks, which are in the fundamental representation, the colour indices are N_C-valued.

The particle momenta featuring in the generic process (3.1) obey the on-shell conditions $p_1^2 = p_2^2 = 0$, $p_3^2 = m_3^2$ and $p_4^2 = m_4^2$. For the kinematical description of the reactions the standard Mandelstam invariants

$$s = (p_1 + p_2)^2 \quad, \quad t = (p_1 - p_3)^2 \qquad \text{and} \qquad u = (p_1 - p_4)^2 \tag{3.2}$$

are used. In the centre-of-mass frame of the final-state particles the absolute value of the final-state momenta can then be written as

$$|\vec{p_3}|_{\text{cm}} \;=\; |\vec{p_4}|_{\text{cm}} \;=\; \frac{1}{2}\kappa\beta\sqrt{s}\,, \tag{3.3}$$

with $\beta = \sqrt{1 - (m_3 + m_4)^2/s}$ defined in Eq. (2.2) and

$$\kappa \;\equiv\; \sqrt{1 - \frac{(m_3 - m_4)^2}{s}}\,. \tag{3.4}$$

The presence of the factor κ is special to the case of unequal masses. As Eq. (3.3) shows, it occurs quite naturally in matrix-element expressions for the processes we consider in this study. We could have defined the variable $\beta' = \kappa\beta$ and taken moments with respect to this variable. Instead we have opted to use the variable β in our calculations in order to

facilitate convolutions underlying the resummation. Because $\log \beta' = \log \beta + \log \kappa$, choosing β' would have resulted in different subleading logarithmic terms. To NLL accuracy these differences in the expressions for the resummed partonic cross sections are cancelled by different terms arising from the convolutions.

In order to present the results for the leading-order partonic cross sections it is helpful to introduce two more shorthand notations:

$$m_+^2 \equiv m_{\tilde{g}}^2 + m_{\tilde{q}}^2 \qquad \text{and} \qquad m_-^2 \equiv m_{\tilde{g}}^2 - m_{\tilde{q}}^2 \,. \tag{3.5}$$

3.2 Colour bases in the s-channel

As discussed in section 2, colour correlations need to be taken into account once NLL soft-gluon resummation is performed for processes involving pair-production of coloured particles. To this end an appropriate colour basis has to be chosen. We have opted to use an s-channel colour basis, which traces the colour flow through the s-channel and has the virtue of rendering the anomalous dimension matrices diagonal at threshold [40, 26, 27, 29].

Since we are dealing with two coloured particles in both initial and final state, the s-channel basis is obtained by performing an s-channel colour decomposition of the reducible two-particle product representations into irreducible ones. For squark-squark and squark-gluino production this amounts to the following decompositions in SU(3):

$$qq \to \tilde{q}\tilde{q}: \qquad \mathbf{3} \otimes \mathbf{3} = \bar{\mathbf{3}} \oplus \mathbf{6} \,,$$

$$qg \to \tilde{q}\tilde{g}: \qquad \mathbf{3} \otimes \mathbf{8} = \mathbf{3} \oplus \bar{\mathbf{6}} \oplus \mathbf{15} \,, \tag{3.6}$$

where the product representations apply to both the initial and final state. In a general $\mathrm{SU}(N_C)$-theory the dimensions of the various representations are of course different, but the number of base tensors for these two processes remains the same.

An economic way to construct the s-channel colour bases for squark-squark and squark-gluino production is to start with an arbitrary complete colour basis of the considered process in terms of which the s-channel base tensors $c_I(a_1, a_2; a_3, a_4)$ can be expressed. Then the s-channel basis can be obtained by simply requiring that a particular base tensor is orthogonal to all other base tensors and projects on itself when contracted in s-channel:

$$\sum_{b,b'} c_I(a_1, a_2; b, b') \, c_{I'}(b, b'; a_3, a_4) = Z \delta_{II'} \, c_I(a_1, a_2; a_3, a_4) \,, \tag{3.7}$$

where Z is an arbitrary normalization constant. A similar procedure was found by the authors of Ref. [29] on the basis of an analysis in terms of Clebsch–Gordon coefficients. This projective construction of the s-channel base tensors constitutes a direct way of obtaining explicit implementations of the irreducible representations on the right-hand side of Eq. (3.6). The minimal requirement for the projective method to work is that the particles in the initial state must be in the same representations as those in the final state, as follows directly from the fact that the labels of the initial state are contracted with those of the final state in Eq. (3.7). This is indeed the case for both the squark-squark and squark-gluino production processes. An example of the calculation of the s-channel colour basis for the $qq \to \tilde{q}\tilde{q}$ process is given in appendix B.

In order to present the s-channel base tensors in the subsequent text, we will need the following $\mathrm{SU}(N_C)$-objects: the singlet colour structures δ_{ab}, where a and b belong to particles in either the adjoint or the fundamental representation, the generators of the fundamental representation T_{ab}^c, the structure constants f_{abc} and the symmetric forms d_{abc}.

3.3 Leading-order partonic cross sections

Having defined all necessary ingredients, we can now present the results for the colour-decomposed $\tilde{q}\tilde{q}$ and $\tilde{q}\tilde{g}$ partonic cross sections at LO. These partonic cross sections are averaged over initial-state spin and colour. The colour-decomposed LO cross sections for the $q\bar{q} \to \tilde{q}\bar{\tilde{q}}$, $gg \to \tilde{q}\bar{\tilde{q}}$, $q\bar{q} \to \tilde{g}\tilde{g}$ and $gg \to \tilde{g}\tilde{g}$ processes, together with their Mellin-moment transforms, can be found in Ref. [27].

3.3.1 Squark-squark production

We consider the process

$$q_{f_1}(a_1, p_1)\, q_{f_2}(a_2, p_2) \;\to\; \tilde{q}(a_3, p_3)\, \tilde{q}(a_4, p_4)\,, \tag{3.8}$$

where the flavours of the initial-state quarks are indicated by f_1, f_2 and all external particles are in the fundamental representation of $\mathrm{SU}(N_C)$. The method described in section 3.2 to obtain a suitable s-channel colour basis yields the following two colour tensors:

$$c_1^{qq} \;=\; \delta_{a_1a_4}\delta_{a_2a_3} - \delta_{a_1a_3}\delta_{a_2a_4} \qquad \text{and} \qquad c_2^{qq} \;=\; \delta_{a_1a_4}\delta_{a_2a_3} + \delta_{a_1a_3}\delta_{a_2a_4}\,. \tag{3.9}$$

The dimensions of the representations spanned by these two base tensors are given by $\dim(R_1^{qq}) = \frac{1}{2}N_C(N_C - 1)$ and $\dim(R_2^{qq}) = \frac{1}{2}N_C(N_C + 1)$. In the SU(3) case this basis coincides up to normalization factors with the base tensors given in Ref. [29] for the $\mathbf{\bar{3}}$ and $\mathbf{6}$ representations. The decomposition of the LO partonic squark-pair cross section in terms of the base tensors (3.9) is given by

$$\sigma_{qq \to \tilde{q}\tilde{q},1}^{(0)} = \frac{\pi\alpha_{\mathrm{s}}^2(N_C^2 - 1)(N_C + 1)}{4N_C^3 s}\left[\frac{2m_{\tilde{g}}^2}{2m_-^2 + s}\,L_1\,\delta_{f_1f_2} - \frac{2m_-^2 + s}{s}\,L_1 - \frac{2m_-^4 + sm_{\tilde{g}}^2}{m_-^4 + sm_{\tilde{g}}^2}\,\beta\right],$$

$$\sigma_{qq \to \tilde{q}\bar{\tilde{q}},2}^{(0)} = \frac{\pi\alpha_{\mathrm{s}}^2(N_C^2 - 1)(N_C - 1)}{4N_C^3 s}\left[\frac{-2m_{\tilde{g}}^2}{2m_-^2 + s}\,L_1\,\delta_{f_1f_2} - \frac{2m_-^2 + s}{s}\,L_1 - \frac{2m_-^4 + sm_{\tilde{g}}^2}{m_-^4 + sm_{\tilde{g}}^2}\,\beta\right],$$

with

$$L_1 \;\equiv\; \log\left(\frac{s + 2m_-^2 - s\beta}{s + 2m_-^2 + s\beta}\right).$$

The quantities β and m_-^2 are defined in Eqs. (2.2) and (3.5), using $m_3 = m_4 = m_{\tilde{q}}$. The occurrence of the Kronecker-delta $\delta_{f_1f_2}$ reflects the fact that for equal-flavoured initial-state quarks extra diagrams contribute. In appendix A we present results for the Mellin-moment transforms of these colour-decomposed LO cross sections.

3.3.2 Squark-gluino production

At the partonic level the $\tilde{q}\tilde{g}$ production process is given by

$$q_{f_1}(a_1, p_1)\, g(a_2, p_2) \;\rightarrow\; \tilde{q}(a_3, p_3)\, \tilde{g}(a_4, p_4)\,. \tag{3.10}$$

The initial and final state of this process involves both a particle in the fundamental representation (q or $\tilde{q}$) and a particle in the adjoint representation (g or $\tilde{g}$). For the s-channel colour decomposition the following three base tensors are used:

$$c_1^{qg} \;=\; \left(T^{a_4}T^{a_2}\right)_{a_3 a_1},$$

$$c_2^{qg} \;=\; \frac{N_C - 2}{N_C}\,\delta_{a_2 a_4}\delta_{a_1 a_3} \;-\; 2 d_{c a_4 a_2}T^c_{a_3 a_1} \;+\; 2\,\frac{N_C - 2}{N_C - 1}\,(T^{a_4}T^{a_2})_{a_3 a_1}\,,$$

$$c_3^{qg} \;=\; \frac{N_C + 2}{N_C}\,\delta_{a_2 a_4}\delta_{a_1 a_3} \;+\; 2 d_{c a_4 a_2}T^c_{a_3 a_1} \;-\; 2\,\frac{N_C + 2}{N_C + 1}\,(T^{a_4}T^{a_2})_{a_3 a_1}\,. \tag{3.11}$$

The dimensions of the representations spanned by these three base tensors are given by $\dim(R_1^{qg}) = N_C$, $\dim(R_2^{qg}) = \frac{1}{2}N_C(N_C+1)(N_C-2)$ and $\dim(R_3^{qg}) = \frac{1}{2}N_C(N_C-1)(N_C+2)$. In the SU(3) case this basis coincides up to normalization factors with the base tensors given in Ref. [29] for the **3**, **6̄** and **15** representations. The decomposition of the LO partonic squark-gluino cross section in terms of the base tensors (3.11) is given by

$$\sigma^{(0)}_{qg\to\tilde{q}\tilde{g},1} = \frac{\alpha_s^2\pi}{(N_C^2-1)s}\left[\left(\frac{2m_{\tilde{g}}^2 m_-^2}{s^2} - \frac{2m_-^4 + s^2 + 2m_-^2 s}{2s^2}N_C^2\right)L_2\right.$$
$$\left. + \frac{m_-^2}{s}\left(\frac{m_-^2-s}{sN_C^2} + \frac{2m_{\tilde{q}}^2}{s}\right)L_3 - \left(\frac{7m_-^2+3s}{4s}N_C^2 - \frac{3m_-^2+s}{2s} + \frac{7m_-^2-s}{4N_C^2 s}\right)\kappa\beta\right],$$

$$\sigma^{(0)}_{qg\to\tilde{q}\tilde{g},2} = \frac{\alpha_s^2\pi(N_C-2)}{(N_C-1)s}\left[\frac{2m_-^2(m_+^2-s)-s^2}{4s^2}L_2 + \frac{m_-^2(m_+^2-s)}{2s^2}L_3 - \frac{m_-^2}{s}\kappa\beta\right],$$

$$\sigma^{(0)}_{qg\to\tilde{q}\tilde{g},3} = \frac{\alpha_s^2\pi(N_C+2)}{(N_C+1)s}\left[\frac{2m_-^2(m_+^2-s)-s^2}{4s^2}L_2 + \frac{m_-^2(m_+^2-s)}{2s^2}L_3 - \frac{m_-^2}{s}\kappa\beta\right],$$

with

$$L_2 = \log\left(\frac{s+m_-^2-\kappa s\beta}{s+m_-^2+\kappa s\beta}\right) \qquad \text{and} \qquad L_3 = \log\left(\frac{s-m_-^2-\kappa s\beta}{s-m_-^2+\kappa s\beta}\right).$$

The quantities β, κ and $m_\pm^2$ are defined in Eqs. (2.2), (3.4) and (3.5), using $m_3 = m_{\tilde{q}}$ and $m_4 = m_{\tilde{g}}$. In appendix A we present results for the Mellin-moment transforms of these colour-decomposed LO cross sections.

3.4 The soft anomalous-dimension matrices

As we reviewed in section 2 below Eq. (2.11), resummation to NLL accuracy requires the anomalous dimensions Γ_{IJ} of the products of Wilson-line operators connected by a base tensor c_I. To this end one must compute the UV divergences from their loop corrections, and from these the renormalization constants Z_{IJ} for these operators. Here we only need

the one-loop corrections. The anomalous dimensions can be computed from the residues of the UV poles in the renormalization constants Z_{IJ} as

$$\Gamma_{IJ} = -\alpha_{\rm s} \frac{\partial}{\partial \alpha_{\rm s}} \operatorname{Res}_{\epsilon \to 0} Z_{IJ}(\alpha_{\rm s}, \epsilon) \,. \tag{3.12}$$

The relevant UV divergences occur in loop corrections to the base tensors c_I [40, 37] due to the Wilson lines. The complete first order correction to c_I can be written as

$$\sum_{ij} \omega^{ij} \mathcal{C}_{IJ}^{ij} c_J \,, \tag{3.13}$$

where i and j denote the eikonal lines between which the gluon is spanned, ω^{ij} is the corresponding kinematic part of the one-loop correction, and $\mathcal{C}_{IJ}^{ij}$ denotes how the base tensors get mixed due to the corrections. At one-loop we can calculate the anomalous dimensions directly from Eq. (3.13)

$$\Gamma_{IJ} = -\sum_{ij} \mathcal{C}_{IJ}^{ij} \operatorname{Res}_{\epsilon \to 0} \omega^{ij} \,. \tag{3.14}$$

The precise form of this function depends on the colour basis chosen. The eikonal integrals that constitute the ω^{ij} can be found in Ref. [40], except for the unequal-mass case that we need for squark-gluino production. The corresponding integral ω^{34} is discussed in appendix D, using the Feynman rules in the eikonal approximation presented in appendix C.

In order to present the results for the soft anomalous dimensions in a compact way, we introduce the following t- and u-channel quantities

$$\Lambda \equiv \frac{1}{2} \left[T(m_3) + T(m_4) + U(m_3) + U(m_4) \right] ,$$

$$\Omega \equiv \frac{1}{2} \left[T(m_3) + T(m_4) - U(m_3) - U(m_4) \right] , \tag{3.15}$$

in terms of the t- and u-channel logarithms[3]

$$T(m) = \log \left(\frac{m^2 - t}{\sqrt{s m^2}} \right) - \frac{1 - i\pi}{2} \qquad \text{and} \qquad U(m) = \log \left(\frac{m^2 - u}{\sqrt{s m^2}} \right) - \frac{1 - i\pi}{2} \,. \tag{3.16}$$

The one-loop soft anomalous-dimension matrices for the $q\bar{q} \to \tilde{q}\bar{\tilde{q}}$, $gg \to \tilde{q}\bar{\tilde{q}}$, $q\bar{q} \to \tilde{g}\tilde{g}$ and $gg \to \tilde{g}\tilde{g}$ processes have been calculated in Ref. [27], where the corresponding values of the $D_{ij \to kl,I}$ coefficients can be found as well.[4]

3.4.1 Soft anomalous dimensions for squark-pair production at one-loop

In the basis (3.9) the one-loop soft anomalous-dimension matrix is given by

$$\bar{\Gamma}_{qq \to \tilde{q}\tilde{q}} = \frac{\alpha_{\rm s}}{2\pi} \begin{pmatrix} C_2(R_1^{qq}) \Lambda - \dfrac{N_C + 1}{N_C} (L_\beta + 1) & -(N_C + 1) \Omega \\[2ex] -(N_C - 1) \Omega & C_2(R_2^{qq}) \Lambda + \dfrac{N_C - 1}{N_C} (L_\beta + 1) \end{pmatrix} , \tag{3.17}$$

---

[3] Note that in the case of equal masses $m_3 = m_4$ the quantities $\Lambda, \Omega, T(m)$ and $U(m)$ reduce to the corresponding quantities $\bar{\Lambda}, \bar{\Omega}, \bar{T}$ and $\bar{U}$ defined in Ref. [27].

[4] Note that Ref. [27] uses a subtraction term different from Eq. (2.11).

with

$$L_{\beta} \;\; = \;\; \frac{1+\beta^2}{2\beta}\left[\log\left(\frac{1-\beta}{1+\beta}\right) + i\pi\right].$$

The coefficients $C_2(R_I^{qq})$ for $I = 1,2$ are the quadratic Casimir invariants belonging to the representations spanned by the base tensors c_I^{qq}:

$$C_2(R_1^{qq}) \;\; = \;\; \frac{(N_C+1)(N_C-2)}{N_C} \qquad \text{and} \qquad C_2(R_2^{qq}) \;\; = \;\; \frac{(N_C-1)(N_C+2)}{N_C}. \qquad (3.18)$$

3.4.2 Soft anomalous dimensions for squark-gluino production at one-loop

In the basis (3.11) the one-loop soft anomalous-dimension matrix is given by

$$\bar{\Gamma}_{qg\to\tilde{q}\tilde{g}} \;\; = \;\; \frac{\alpha_{\mathrm{s}}}{2\pi}\begin{pmatrix} \bar{\Gamma}_{11,qg} & \dfrac{4N_C^2(N_C-2)}{(N_C^2-1)(N_C-1)}\,\Omega & \dfrac{4N_C^2(N_C+2)}{(N_C^2-1)(N_C+1)}\,\Omega \\[2.5ex] \frac{1}{2}\,\Omega & \bar{\Gamma}_{22,qg} & \dfrac{N_C(N_C+2)}{N_C+1}\,\Omega \\[2.5ex] \frac{1}{2}\,\Omega & \dfrac{N_C(N_C-2)}{N_C-1}\,\Omega & \bar{\Gamma}_{33,qg} \end{pmatrix}, \qquad (3.19)$$

with

$$\bar{\Gamma}_{11,qg} \;\; = \;\; C_2(R_1^{qg})\,\Lambda \;+\; \left[C_F + \frac{1}{C_F}\right]\Omega \;-\; \frac{N_C^2+1}{2N_C}\left[T(m_{\tilde{q}}) - T(m_{\tilde{g}})\right] \;-\; N_C\left(L_{v_3,v_4}+1\right),$$

$$\bar{\Gamma}_{22,qg} \;\; = \;\; C_2(R_2^{qg})\,\Lambda \;+\; \left[C_F - \frac{1}{N_C-1}\right]\Omega \;-\; \frac{N_C^2+1}{2N_C}\left[T(m_{\tilde{q}}) - T(m_{\tilde{g}})\right] \;-\; \left(L_{v_3,v_4}+1\right),$$

$$\bar{\Gamma}_{33,qg} \;\; = \;\; C_2(R_3^{qg})\,\Lambda \;+\; \left[C_F - \frac{1}{N_C+1}\right]\Omega \;-\; \frac{N_C^2+1}{2N_C}\left[T(m_{\tilde{q}}) - T(m_{\tilde{g}})\right] \;+\; \left(L_{v_3,v_4}+1\right),$$

$$(3.20)$$

where

$$L_{v_3,v_4} \;\; = \;\; \frac{\kappa^2+\beta^2}{2\kappa\beta}\left[\log\left(\frac{\kappa-\beta}{\kappa+\beta}\right) + i\pi\right]. \qquad (3.21)$$

The explicit derivation of Eq. (3.21) is presented in appendix D. The coefficients $C_2(R_I^{qg})$ for $I = 1,2,3$ are the quadratic Casimir invariants belonging to the representations spanned by the base tensors c_I^{qg}:

$$C_2(R_1^{qg}) \;\; = \;\; \frac{N_C^2-1}{2N_C} \;\; \equiv \;\; C_F, \qquad C_2(R_2^{qg}) \;\; = \;\; \frac{(N_C-1)(3N_C+1)}{2N_C}$$

$$\text{and} \qquad C_2(R_3^{qg}) \;\; = \;\; \frac{(N_C+1)(3N_C-1)}{2N_C}. \qquad (3.22)$$

3.4.3 The threshold limit

At the production threshold, where $\beta \to 0$, the soft anomalous-dimension matrices become diagonal by virtue of using an s-channel basis. In addition, the diagonal components become proportional to the total colour charge of the heavy-particle pair produced at threshold:

$$D_{ij \to kl, I} = -C_2(R_I^{ij}),\qquad(3.23)$$

with $C_2(R_I^{ij})$ as given in equation (3.18) for squark-pair production and in equation (3.22) for squark-gluino production. In the SU(3) case the $D_{ij \to kl, I}$ coefficients for squark-pair production are given by

$$\{D_{qq \to \tilde{q}\tilde{q}, I}\} = \{-4/3, -10/3\},$$

while for the squark-gluino production process they are

$$\{D_{qg \to \tilde{q}\tilde{g}, I}\} = \{-4/3, -10/3, -16/3\}.$$

4. Numerical results

In this section we present numerical results for the NLL-resummed cross sections matched with the complete NLO results for squark and gluino pair-production at both the Tevatron ($\sqrt{S} = 1.96$ TeV) and the LHC ($\sqrt{S} = 14$ TeV). The matching is performed according to Eq. (2.13). From now on we refer to the matched cross sections as NLL+NLO cross sections. We also compare the NLL+NLO predictions with the corresponding NLO results. The NLO cross sections are calculated using the publicly available PROSPINO code [44], based on the calculations presented in Refs. [14, 15, 16]. As described in detail in Ref. [16], the QCD coupling α_s and the parton distribution functions at NLO are defined in the $\overline{\text{MS}}$ scheme with five active flavours. The masses of squarks and gluinos are renormalized in the on-shell scheme, and the SUSY particles are decoupled from the running of α_s and the parton distribution functions. As already discussed in previous sections, no top-squark final states are considered. We sum over squarks with both chiralities ($\tilde{q}_L$ and $\tilde{q}_R$), which are taken as mass degenerate, and include the charge-conjugated processes in the numerical predictions. For convenience we define the average mass of the sparticle pair $m \equiv (m_3 + m_4)/2$, which reduces to the squark and gluino mass for $\tilde{q}\bar{\tilde{q}}$, $\tilde{q}\tilde{q}$ and $\tilde{g}\tilde{g}$ final states, respectively. The renormalization and factorization scales μ are taken to be equal. In order to evaluate hadronic cross sections we use the 2008 NLO MSTW parton distribution functions [43] with the corresponding $\alpha_s(M_Z^2) = 0.120$. The numerical results have been obtained with two independent computer codes.

We first discuss the scale dependence of the NLL+NLO matched cross section for the separate processes $p\bar{p} \to \tilde{q}\bar{\tilde{q}}, \tilde{q}\tilde{q}, \tilde{q}\tilde{g}, \tilde{g}\tilde{g} + X$ at the Tevatron. Figure 1 shows the NLO and NLL+NLO cross sections for $m_{\tilde{q}} = m_{\tilde{g}} = m = 500$ GeV as a function of the renormalization and factorization scale μ. The value of μ is varied around the central scale $\mu_0 = m$ from $\mu = \mu_0/10$ up to $\mu = 5\,\mu_0$. As anticipated, we observe a reduction of the scale dependence when going from NLO to NLL+NLO, in particular for $\tilde{g}\tilde{g}$ and $\tilde{q}\tilde{g}$ production (Figs. 1b and 1d, respectively). In the case of squark pair-production, on the other hand, the scale

reduction due to soft-gluon resummation is moderate (see Figs. 1a and 1c). We note that the gluino-pair production cross section (Fig. 1b) is rather small for this particular choice of masses because of a suppression of the LO $q\bar{q} \to \tilde{g}\tilde{g}$ amplitude proportional to $m_{\tilde{g}}^2 - m_{\tilde{q}}^2$ near threshold (cf. Eq. (55) of Ref. [16]).

At the central scale $\mu = \mu_0 = m$ the cross-section predictions are in general enhanced by soft-gluon resummation. The relative K-factor $K_{\mathrm{NLL}} - 1 \equiv \sigma_{\mathrm{NLL+NLO}}/\sigma_{\mathrm{NLO}} - 1$ at the Tevatron is displayed in Fig. 2 for squark and gluino masses in the range between 200 GeV and 600 GeV. We show results for various mass ratios $r \equiv m_{\tilde{g}}/m_{\tilde{q}}$. The soft-gluon corrections are moderate for $\tilde{q}\bar{\tilde{q}}$ production (Fig. 2a), but reach values up to 27%, 29% and 60% for $\tilde{g}\tilde{g}$, $\tilde{q}\tilde{q}$ and $\tilde{q}\tilde{g}$ final states, respectively, in the range of r we consider. Because of the increasing importance of the threshold region, the corrections in general become larger for increasing sparticle masses. The strong r-dependence of K_{NLL} for gluino-pair production in Fig. 2b is driven by the r-dependence of the NLO cross sections for $q\bar{q} \to \tilde{g}\tilde{g}$. The large effect of soft-gluon resummation for $\tilde{q}\tilde{g}$ and $\tilde{g}\tilde{g}$ production can be mostly attributed to the importance of gluon initial states for these processes. Furthermore, the presence of gluinos in the final state results in enhancement of the NLL contributions [27], since in this case the Casimir invariants that enter Eq. (2.8) reach higher values than for processes involving only squarks. The substantial value of K_{NLL} for $\tilde{q}\bar{\tilde{q}}$ production at the Tevatron is a consequence of the behaviour of the corresponding NLO corrections, which strongly decrease with increasing squark mass [16].

We now turn to the discussion of pair production of squarks and gluinos at the LHC, i.e. $pp \to \tilde{q}\bar{\tilde{q}}, \tilde{q}\tilde{q}, \tilde{q}\tilde{g}, \tilde{g}\tilde{g} + X$. The results for the processes $pp \to \tilde{q}\bar{\tilde{q}}$ and $pp \to \tilde{g}\tilde{g}$ agree with those presented in Refs. [26, 27], while the predictions for $pp \to \tilde{q}\tilde{q}$ and $pp \to \tilde{q}\tilde{g}$ are new. In Fig. 3 the cross sections are shown for squark and gluino masses $m_{\tilde{q}} = m_{\tilde{g}} = m = 1$ TeV as a function of the common renormalization and factorization scale μ. The scale uncertainty of the theoretical prediction is reduced at NLL+NLO. Similarly to the Tevatron case, soft-gluon resummation is most significant for gluino-pair production and squark-gluino production. For those processes, the relative K-factor $K_{\mathrm{NLL}} - 1$ reaches 35% for gluino-pair production and 18% for squark-gluino production at the highest accessible sparticle masses around 3 TeV (see Figs. 4b and 4d). The r-dependence of K_{NLL} for gluino-pair production is again driven by the r-dependence of the NLO cross section, discussed in Ref. [16].

Representative values for the NLO and NLL+NLO cross sections at the Tevatron and the LHC are collected in Tables 1 and 2 for equal squark and gluino masses.

The impact of the NLL resummation on the cross section for inclusive squark and gluino production, i.e. $p\bar{p}/pp \to \tilde{q}\bar{\tilde{q}} + \tilde{q}\tilde{q} + \tilde{q}\tilde{g} + \tilde{g}\tilde{g} + X$, can be inferred from the inclusive K-factor displayed in Fig. 5. The pattern exhibited in Fig. 5 can be understood from the relative importance of the $\tilde{q}\bar{\tilde{q}}, \tilde{q}\tilde{q}, \tilde{q}\tilde{g}$ and $\tilde{g}\tilde{g}$ final states and from their individual K-factors as shown in Figs. 2 and 4. At $m_{\tilde{q}} = m_{\tilde{g}} \approx 400$ GeV, for example, the inclusive cross section at the Tevatron (Fig. 5a) is built up from the individual final states in the ratio $\tilde{q}\bar{\tilde{q}} : \tilde{g}\tilde{g} : \tilde{q}\tilde{g} : \tilde{q}\bar{\tilde{q}} \approx 1 : 3.6 : 14 : 32$, as can be read off from Table 1. Owing to the large NLL corrections for the $\tilde{q}\tilde{g}$ final state, the resulting inclusive K-factor K_{NLL} is approximately 1.1. At $m_{\tilde{q}} = m_{\tilde{g}} = 600$ GeV the correction to the inclusive cross section at

the Tevatron due to NLL resummation can be as high as 18%. The inclusive corrections are smaller at the LHC for sparticle masses below 3 TeV (see Fig. 5b). Given the sparticle mass ranges that we consider, this is consistent with the fact that the distance from threshold, i.e. the value of the variable $1 - \rho = 1 - 4m^2/S$, is on average larger at the LHC than at the Tevatron.

In Figs. 6a and 6b we show for the Tevatron and LHC, respectively, the resummed NLL+NLO total cross section for inclusive squark and gluino production as a function of the average sparticle mass m. For illustration we show these results for the choice $m_{\tilde{q}} = m_{\tilde{g}}$. The error bands indicate the theoretical uncertainty of the NLL+NLO total cross section due to the scale variation in the range $m/2 \leq \mu \leq 2m$. The results presented in Fig. 6 are the most accurate theoretical predictions currently available for the above processes. The reduction of the theoretical error due to variation of the common factorization and renormalization scale μ between $\mu = m/2$ and $\mu = 2m$ is illustrated in Fig. 7a for the Tevatron and in Fig. 7b for the LHC. Both at the Tevatron and at the LHC, soft-gluon resummation leads to a significant reduction in this part of the theoretical uncertainty.

5. Conclusions

We have performed the NLL resummation of soft gluon emission for squark and gluino hadroproduction. Explicit analytical results are presented for the anomalous dimension matrices and the colour-decomposed LO cross sections in x and N-space for the $\tilde{q}\tilde{q}$ and $\tilde{q}\tilde{g}$ final states. We provide NLO+NLL matched numerical predictions for all pair-production processes of coloured sparticles at the Tevatron and the LHC. The NLL corrections lead to a significant reduction of the scale dependence and, in general, increase the NLO cross sections. The effect of soft-gluon resummation is most pronounced for processes with initial-state gluons and final-state gluinos, which involve a large colour charge. Specifically, at the Tevatron we find an increase of the cross-section prediction of up to 40% at sparticle masses around 500 GeV when going from NLO to NLL+NLO, depending in detail on the final state and the ratio of squark to gluino masses. For the inclusive sparticle cross section at the Tevatron, summed over all pair-production processes for squarks and gluinos, the enhancement can be as large as approximately 15% in the mass range up to 500 GeV, probed by current experimental searches. At the LHC, the NLL corrections are particularly significant for squark-gluino production and gluino-pair production, reaching approximately 20% and 30%, respectively, for sparticle masses around 3 TeV. Both at the Tevatron and at the LHC, the inclusion of NLL corrections leads to a reduction of the scale dependence over the full mass range that will be probed by experiments. In addition, the NLL corrections lead to a significant enhancement of the NLO cross-section predictions for heavy sparticles. The NLL+NLO matched predictions presented in this paper should thus be used to interpret current and future searches for supersymmetry at the Tevatron and the LHC.

Acknowledgments
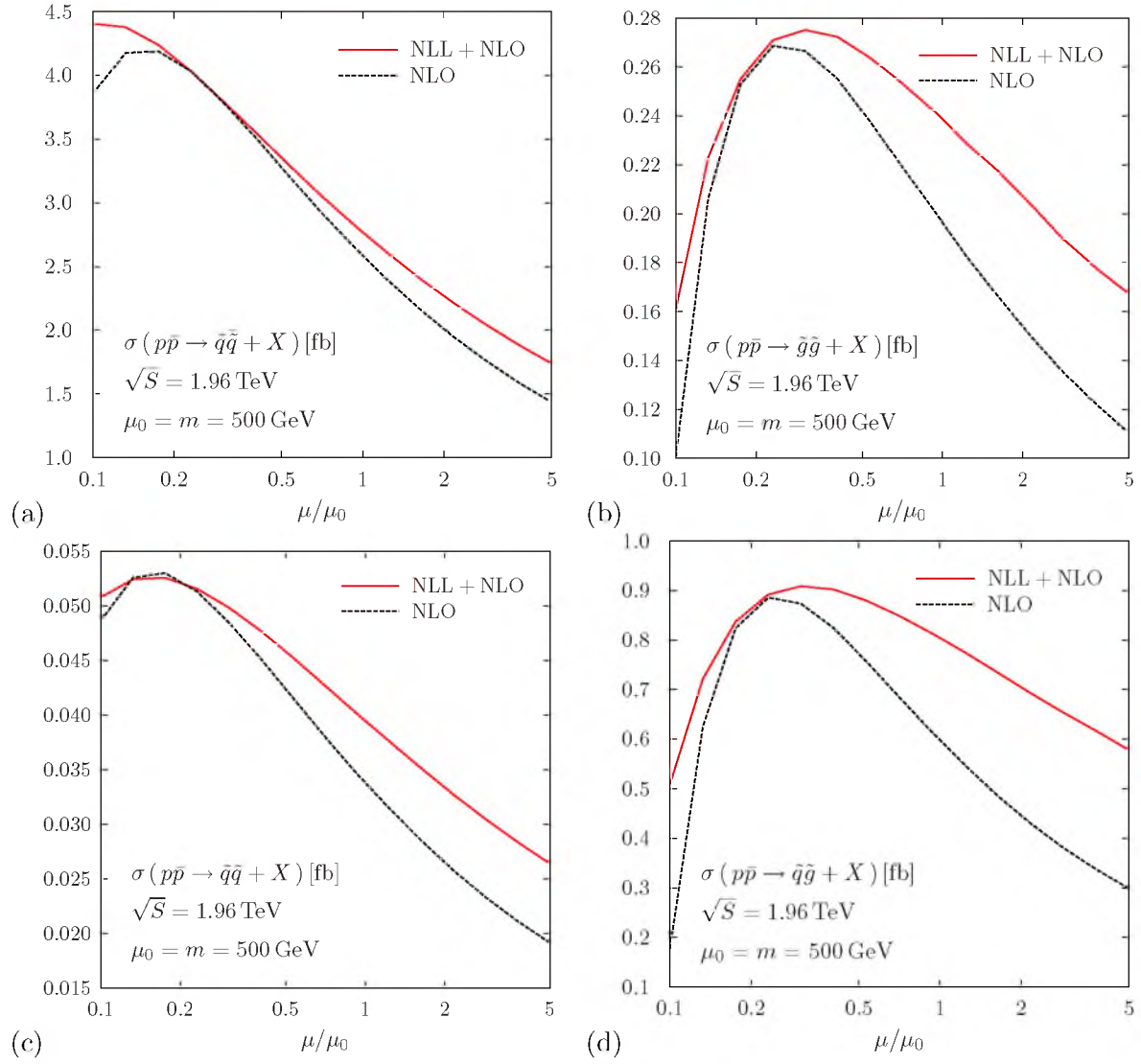
Figure 1: The scale dependence of the NLL+NLO and the NLO total cross sections for squark and gluino pair-production processes at the Tevatron. The squark and gluino masses have been set to $m_{\tilde{q}} = m_{\tilde{g}} = m = 500$ GeV.
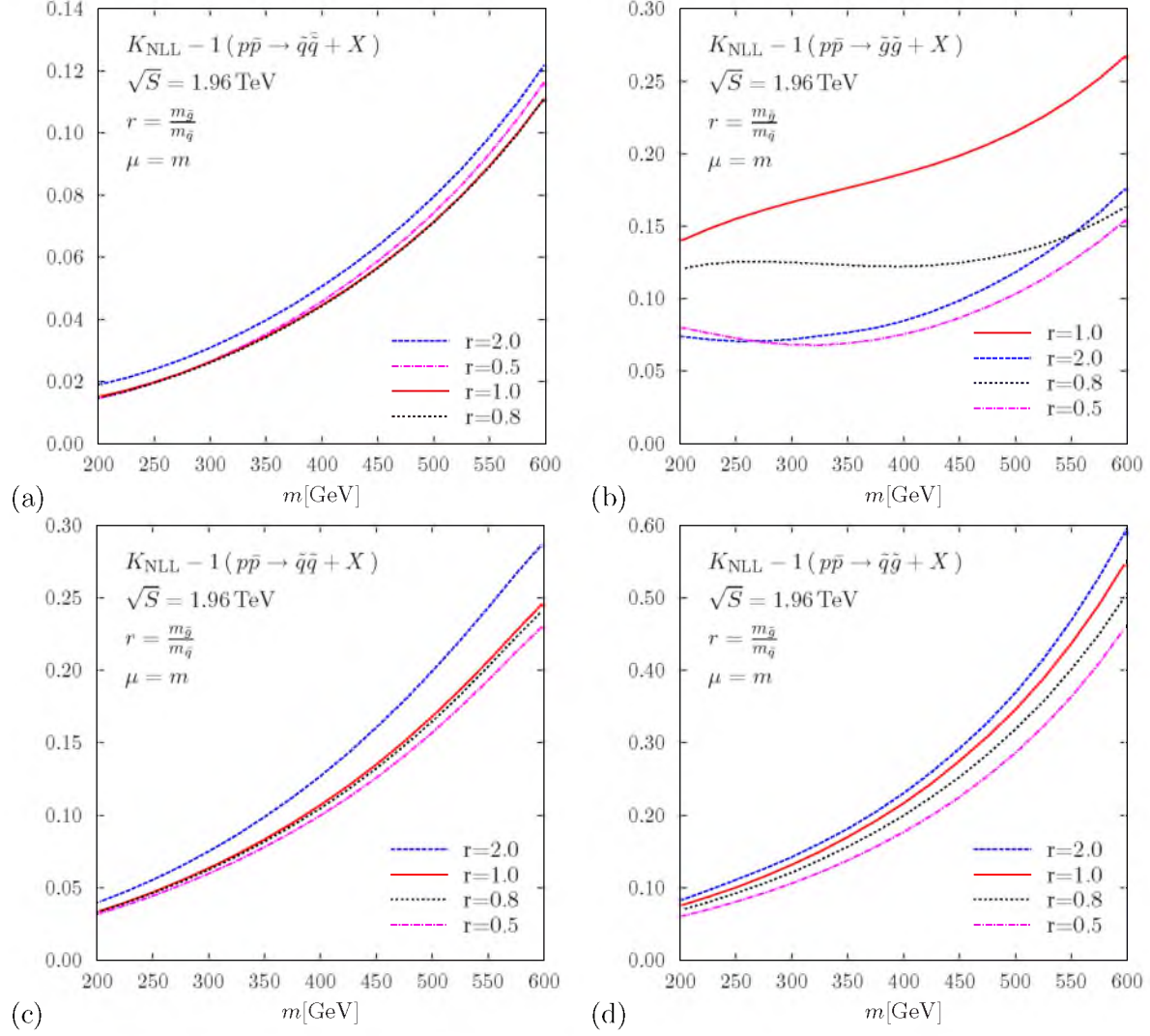
Figure 2: The relative NLL K-factor $K_{\mathrm{NLL}} - 1 = \sigma_{\mathrm{NLL+NLO}}/\sigma_{\mathrm{NLO}} - 1$ for squark and gluino pair-production processes at the Tevatron as a function of the average sparticle mass m. Shown are results for various mass ratios $r = m_{\tilde{g}}/m_{\tilde{q}}$.
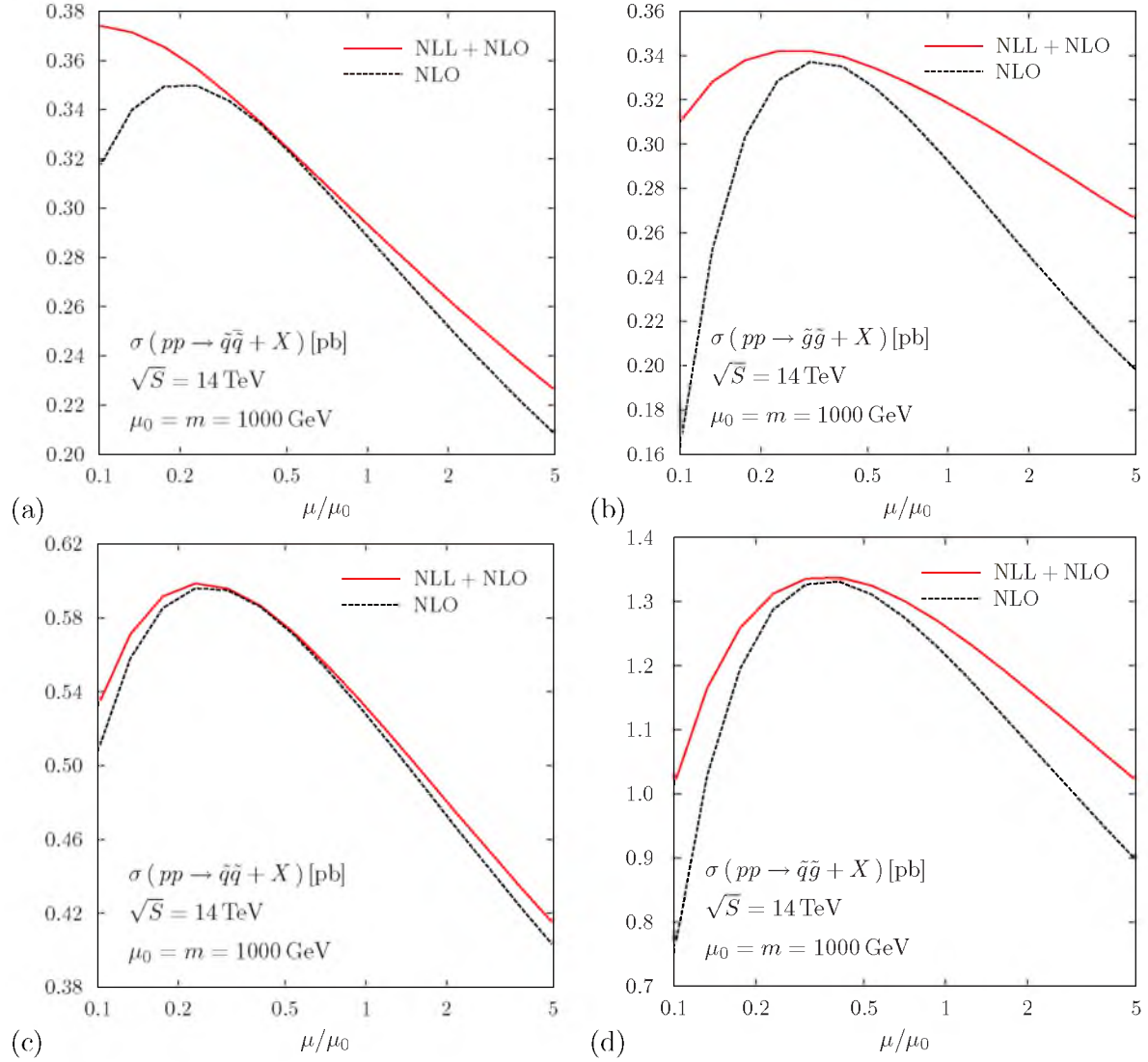
Figure 3: The scale dependence of the NLL+NLO and the NLO total cross sections for squark and gluino pair-production processes at the LHC. The squark and gluino masses have been set to $m_{\tilde{q}} = m_{\tilde{g}} = m = 1$ TeV.
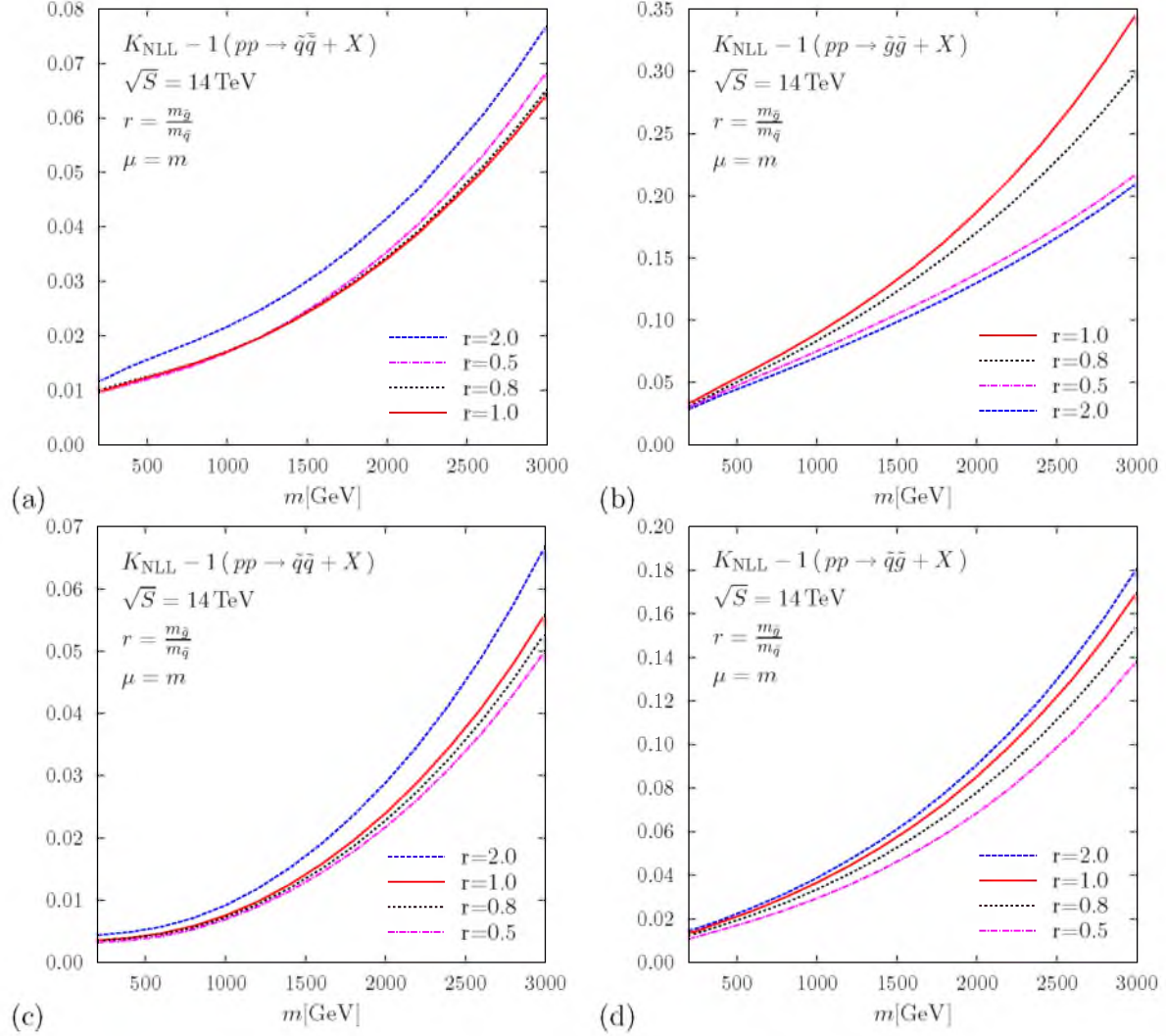
Figure 4: The relative NLL K-factor $K_{\mathrm{NLL}} - 1 = \sigma_{\mathrm{NLL+NLO}}/\sigma_{\mathrm{NLO}} - 1$ for squark and gluino pair-production processes at the LHC as a function of the average sparticle mass m. Shown are results for various mass ratios $r = m_{\tilde{g}}/m_{\tilde{q}}$.
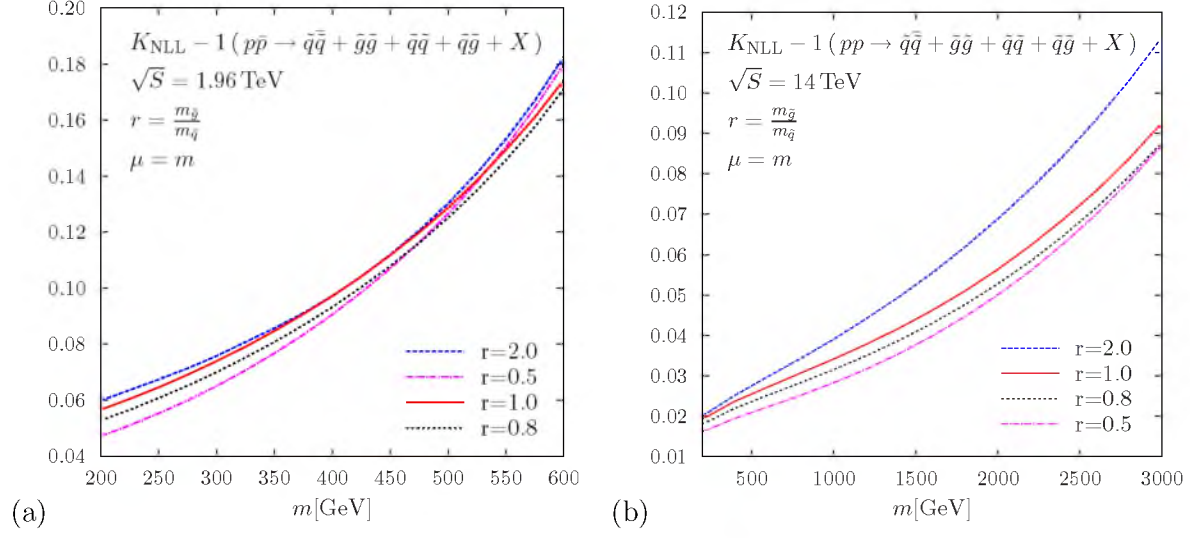
Figure 5: The relative NLL K-factor $K_{\mathrm{NLL}} - 1 = \sigma_{\mathrm{NLL+NLO}}/\sigma_{\mathrm{NLO}} - 1$ for the inclusive squark and gluino pair-production cross section, $p\bar{p}/pp \to \tilde{q}\tilde{q} + \tilde{q}\bar{\tilde{q}} + \tilde{q}\tilde{g} + \tilde{g}\tilde{g} + X$, at the Tevatron (a) and the LHC (b) as a function of the average sparticle mass m. Shown are results for various mass ratios $r = m_{\tilde{g}}/m_{\tilde{q}}$.

Figure 6: The NLL+NLO cross section for inclusive squark and gluino pair-production, $p\bar{p}/pp \to \tilde{q}\tilde{q} + \tilde{q}\bar{\tilde{q}} + \tilde{q}\tilde{g} + \tilde{g}\tilde{g} + X$, at the Tevatron (a) and the LHC (b) as a function of the average sparticle mass m. Shown are results for the mass ratio $r = m_{\tilde{g}}/m_{\tilde{q}} = 1$. The error band corresponds to a variation of the common renormalization and factorization scale in the range $m/2 \leq \mu \leq 2m$.
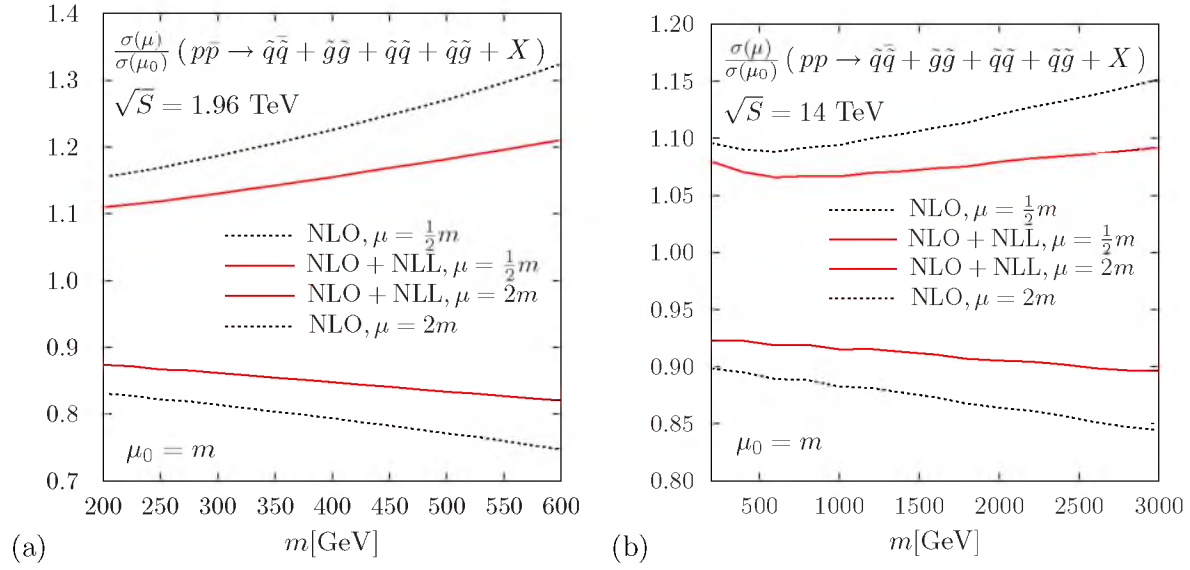
Figure 7: Scale dependence of the NLL+NLO and NLO cross sections for inclusive squark and gluino pair-production, $p\bar{p}/pp \to \tilde{q}\tilde{q} + \tilde{q}\bar{\tilde{q}} + \tilde{q}\tilde{g} + \tilde{g}\tilde{g} + X$, at the Tevatron (a) and the LHC (b) as a function of the average sparticle mass m. Shown are results for the mass ratio $r = m_{\tilde{g}}/m_{\tilde{q}} = 1$. The upper two curves correspond to the common renormalization and factorization scale set to $\mu = m/2$, the lower two curves to $\mu = 2m$.

$p\bar{p} \to \tilde{q}\bar{\tilde{q}}$ at $\sqrt{S} = 1.96\,\mathrm{TeV}$ (r=1.0)

$m_{\tilde{q}}$ [GeV]	200	300	400	500	600
σ_{NLO} [pb]	1.28×10^1	7.35×10^{-1}	4.70×10^{-2}	2.59×10^{-3}	9.79×10^{-5}
$\sigma_{\mathrm{NLL+NLO}}$ [pb]	1.30×10^1	7.55×10^{-1}	4.91×10^{-2}	2.77×10^{-3}	1.09×10^{-4}
$\mathrm{K}_{\mathrm{NLL}} - 1$	0.016	0.026	0.045	0.071	0.11

$p\bar{p} \to \tilde{g}\tilde{g}$ at $\sqrt{S} = 1.96\,\mathrm{TeV}$ (r=1.0)

$m_{\tilde{g}}$ [GeV]	200	300	400	500	600
σ_{NLO} [pb]	3.72	1.07×10^{-1}	4.61×10^{-3}	1.96×10^{-4}	6.01×10^{-6}
$\sigma_{\mathrm{NLL+NLO}}$ [pb]	4.24	1.24×10^{-1}	5.47×10^{-3}	2.38×10^{-4}	7.62×10^{-6}
$\mathrm{K}_{\mathrm{NLL}} - 1$	0.14	0.17	0.19	0.22	0.27

$p\bar{p} \to \tilde{q}\tilde{q}$ at $\sqrt{S} = 1.96\,\mathrm{TeV}$ (r=1.0)

$m_{\tilde{q}}$ [GeV]	200	300	400	500	600
σ_{NLO} [pb]	1.81	4.78×10^{-2}	1.39×10^{-3}	3.38×10^{-5}	5.66×10^{-7}
$\sigma_{\mathrm{NLL+NLO}}$ [pb]	1.87	5.09×10^{-2}	1.54×10^{-3}	3.95×10^{-5}	7.06×10^{-7}
$\mathrm{K}_{\mathrm{NLL}} - 1$	0.033	0.064	0.11	0.17	0.25

$p\bar{p} \to \tilde{q}\tilde{g}$ at $\sqrt{S} = 1.96\,\mathrm{TeV}$ (r=1.0)

m [GeV]	200	300	400	500	600
σ_{NLO} [pb]	1.43×10^1	4.44×10^{-1}	1.71×10^{-2}	5.98×10^{-4}	1.46×10^{-5}
$\sigma_{\mathrm{NLL+NLO}}$ [pb]	1.54×10^1	5.03×10^{-1}	2.09×10^{-2}	8.05×10^{-4}	2.27×10^{-5}
$\mathrm{K}_{\mathrm{NLL}} - 1$	0.075	0.13	0.22	0.35	0.55

Table 1: The NLL+NLO and NLO cross sections for the squark and gluino pair-production processes at the Tevatron. Shown are results f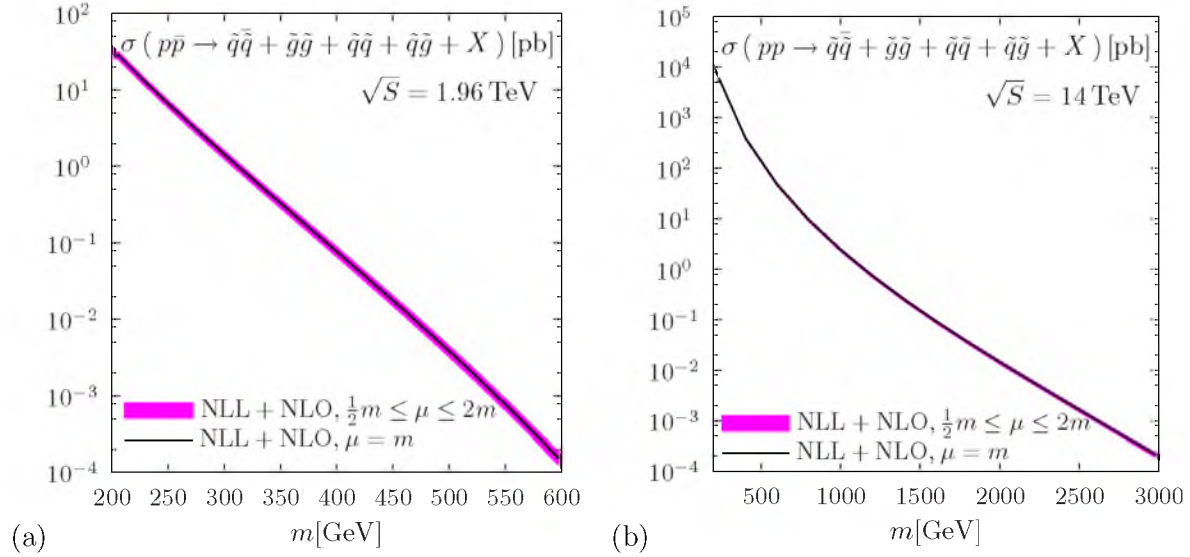or the mass ratio $r = m_{\tilde{g}}/m_{\tilde{q}} = 1$. The common renormalization and factorization scale has been set to m.

$pp \to \tilde{q}\tilde{q}$ at $\sqrt{S} = 14\,\mathrm{TeV}$ (r=1.0)

$m_{\tilde{q}}$ [GeV]	200	500	1000	2000	3000
σ_{NLO} [pb]	1.30×10^3	1.60×10^1	2.89×10^{-1}	1.11×10^{-3}	7.13×10^{-6}
$\sigma_{\mathrm{NLL+NLO}}$ [pb]	1.31×10^3	1.61×10^1	2.93×10^{-1}	1.14×10^{-3}	7.59×10^{-6}
$\mathrm{K_{NLL}} - 1$	0.010	0.012	0.017	0.034	0.064

$pp \to \tilde{g}\tilde{g}$ at $\sqrt{S} = 14\,\mathrm{TeV}$ (r=1.0)

$m_{\tilde{g}}$ [GeV]	200	500	1000	2000	3000
σ_{NLO} [pb]	3.74×10^3	2.85×10^1	2.92×10^{-1}	5.82×10^{-4}	2.68×10^{-6}
$\sigma_{\mathrm{NLL+NLO}}$ [pb]	3.86×10^3	3.00×10^1	3.18×10^{-1}	6.91×10^{-4}	3.62×10^{-6}
$\mathrm{K_{NLL}} - 1$	0.033	0.054	0.089	0.19	0.35

$pp \to \tilde{q}\bar{\tilde{q}}$ at $\sqrt{S} = 14\,\mathrm{TeV}$ (r=1.0)

$m_{\tilde{q}}$ [GeV]	200	500	1000	2000	3000
σ_{NLO} [pb]	5.45×10^2	1.34×10^1	5.28×10^{-1}	6.48×10^{-3}	1.18×10^{-4}
$\sigma_{\mathrm{NLL+NLO}}$ [pb]	5.46×10^2	1.34×10^1	5.32×10^{-1}	6.64×10^{-3}	1.25×10^{-4}
$\mathrm{K_{NLL}} - 1$	0.003	0.004	0.008	0.024	0.056

$pp \to \tilde{q}\tilde{g}$ at $\sqrt{S} = 14\,\mathrm{TeV}$ (r=1.0)

m [GeV]	200	500	1000	2000	3000
σ_{NLO} [pb]	4.86×10^3	6.55×10^1	1.22	5.49×10^{-3}	4.96×10^{-5}
$\sigma_{\mathrm{NLL+NLO}}$ [pb]	4.92×10^3	6.69×10^1	1.26	5.96×10^{-3}	5.80×10^{-5}
$\mathrm{K_{NLL}} - 1$	0.013	0.021	0.037	0.085	0.17

Table 2: The NLL+NLO and NLO cross sections for the squark and gluino pair-production processes at the LHC. Shown are results for the mass ratio $r = m_{\tilde{g}}/m_{\tilde{q}} = 1$. The common renormalization and factorization scale has been set to m.

A. Leading-order N-space cross sections for $\tilde{q}\tilde{q}$ and $\tilde{q}\tilde{g}$ production

In this appendix we present the analytical results for the Mellin transforms of the LO cross sections for $\tilde{q}\tilde{q}$ and $\tilde{q}\tilde{g}$ production. The cross sections are colour-decomposed in SU(3) according to the procedure described in section 3. The Mellin-transformed LO cross sections for the $\tilde{q}\bar{\tilde{q}}$ and $\tilde{g}\tilde{g}$ final states can be found in [27].

The expressions for the colour-decomposed LO N-space cross sections for the process $q_{f_1}q_{f_2} \to \tilde{q}\tilde{q}$ are given by

$$
\tilde{\sigma}^{(0)}_{qq \to \tilde{q}\tilde{q},1}(N) = \frac{\alpha_s^2 \pi}{27 m_{\tilde{q}}^2} \left[- \delta_{f_1 f_2} H_N - \frac{4 B_N G_N}{2N+3} \left(N + \frac{2r^2}{r^2+1} \frac{1}{N+2} \right) \right.
$$

$$
\left. + 2 B_N \frac{N^2 + 2N + 2}{(N+1)(N+2)} \right], \tag{A.1}
$$

$$
\tilde{\sigma}^{(0)}_{qq \to \tilde{q}\tilde{q},2}(N) = \frac{\alpha_s^2 \pi}{27 m_{\tilde{q}}^2} \left[\delta_{f_1 f_2} \frac{H_N}{2} - \frac{2 B_N G_N}{2N+3} \left(N + \frac{2r^2}{r^2+1} \frac{1}{N+2} \right) \right.
$$

$$
\left. + B_N \frac{N^2 + 2N + 2}{(N+1)(N+2)} \right], \tag{A.2}
$$

whereas for the process $qg \to \tilde{q}\tilde{g}$ they read

$$
\tilde{\sigma}^{(0)}_{qg \to \tilde{q}\tilde{g},1}(N) = \frac{\alpha_s^2 \pi}{8 m_{\tilde{q}}^2} \left[\frac{9 B_{N+1} P_{N+1}^- (1-r)}{(r+1)^3} - \frac{9 B_N P_N^-}{2(r+1)^2} + \frac{B_{N+2} P_{N+2}^- (7r^2 - 9)(1-r)}{(r+1)^5} \right.
$$

$$
+ \frac{B_{N+1} P_{N+1}^+ (1-r)}{9(r+1)^3} - \frac{B_{N+2} P_{N+2}^+ (r^2 + 17)(1-r)}{9(r+1)^5}
$$

$$
\left. + \frac{130 B_{N+1} K_{N+1} (1-r)}{9(r+1)^3} - \frac{56 B_N K_N}{9(r+1)^2} \right], \tag{A.3}
$$

$$
\tilde{\sigma}^{(0)}_{qg \to \tilde{q}\tilde{g},2}(N) = \frac{\alpha_s^2 \pi}{8 m_{\tilde{q}}^2} \left[\frac{2 B_{N+1} P_{N+1}^- (1-r)}{(r+1)^3} - \frac{B_N P_N^-}{(r+1)^2} - \frac{2 B_{N+2} P_{N+2}^- (r^2 + 1)(1-r)}{(r+1)^5} \right.
$$

$$
+ \frac{2 B_{N+1} P_{N+1}^+ (1-r)}{(r+1)^3} - \frac{2 B_{N+2} P_{N+2}^+ (r^2 + 1)(1-r)}{(r+1)^5}
$$

$$
\left. + \frac{4 B_{N+1} K_{N+1} (1-r)}{(r+1)^3} \right], \tag{A.4}
$$

$$
\tilde{\sigma}^{(0)}_{qg \to \tilde{q}\tilde{g},3}(N) = \frac{5}{2} \tilde{\sigma}^{(0)}_{qg \to \tilde{q}\tilde{g},2}(N) . \tag{A.5}
$$

We have used the following abbreviations:

$$B_N \equiv \beta(N+1, 1/2)\,,$$

$$G_N \equiv {}_2F_1\left(1, 1/2, N+5/2, \left(\frac{r^2-1}{r^2+1}\right)^2\right)\,,$$

$$P_N^\pm \equiv \frac{-1}{N+1}\, {}_2F_1\left(1/2, N+1, N+3/2, \left(\frac{1-r}{1+r}\right)^2\right)$$

$$\pm \left(\frac{1-r}{r+1}\right)\frac{1}{N+3/2}\, {}_2F_1\left(1/2, N+2, N+5/2, \left(\frac{1-r}{1+r}\right)^2\right)\,,$$

$$K_N \equiv \frac{1}{2N+3}\, {}_2F_1\left(-1/2, N+1, N+5/2, \left(\frac{1-r}{1+r}\right)^2\right)\,,$$

$$H_N \equiv \int_0^1 dz \frac{z^{N+1}}{\frac{1}{r^2} - \left(\frac{1-r^2}{2r^2}\right)z}\log\left(\frac{2(1+\sqrt{1-z}) + (r^2-1)z}{2(1-\sqrt{1-z}) + (r^2-1)z}\right)\,,$$

(A.6)

with ${}_2F_1(\lambda, \mu, \nu, \xi)$ the hypergeometric function, $\beta(\mu, \nu)$ the beta function and $r = m_{\tilde{g}}/m_{\tilde{q}}$. For the numerical evaluation of H_N we use the expansion

$$H_N = \frac{2r^2}{1+r^2}\sum_{m=0}^{\infty}\left(\frac{r^2-1}{1+r^2}\right)^m \frac{1}{1+m}\sum_{k=0}^{m}\frac{(-1)^k}{\beta(k+1, m-k+1)}$$

$$\times \left[\frac{\beta(k+N+2, 1/2)}{k+N+2} - 2\left(\frac{r^2-1}{1+r^2}\right)\beta(k+N+2, 3/2)\right.$$

$$\left. {}_2F_1\left(1, 1/2, k+N+7/2, \left(\frac{1-r^2}{1+r^2}\right)^2\right)\right]\,.$$

(A.7)

B. Construction of the *s*-channel colour basis: an example

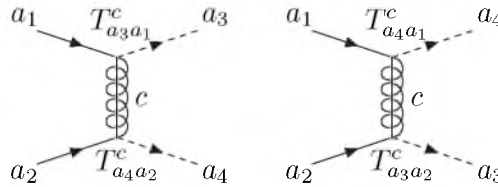**Figure 8:** The LO diagrams that contribute to squark-pair production.

For the process $qq \to \tilde{q}\tilde{q}$ we explicitly show how to derive the *s*-channel colour basis given in Eq. (3.9). The same steps can be used to obtain the basis given in Eq. (3.11) for the $qg \to \tilde{q}\tilde{g}$ process, although the calculations are more tedious in that case.

As a starting point we take the colour structures that occur in the LO $qq \to \tilde{q}\tilde{q}$ process displayed in Fig. 8. Using the conventions introduced in section 3.1 these are:

$$T^c_{a_3 a_1} T^c_{a_4 a_2} = \frac{1}{2}\left(\delta_{a_3 a_2}\delta_{a_4 a_1} - \frac{1}{N_C}\delta_{a_3 a_1}\delta_{a_4 a_2}\right),$$

$$T^c_{a_3 a_2} T^c_{a_4 a_1} = \frac{1}{2}\left(\delta_{a_3 a_1}\delta_{a_4 a_2} - \frac{1}{N_C}\delta_{a_3 a_2}\delta_{a_4 a_1}\right),$$

where c is a summation index in the adjoint representation. For convenience these colour structures have been rewritten in terms of the t and u-channel singlet structures $\delta_{a_3 a_1}\delta_{a_4 a_2}$ and $\delta_{a_3 a_2}\delta_{a_4 a_1}$. It is clear from this expression that two independent singlet structures occur. Since the two-particle reducible product representation $\mathbf{3}\otimes\mathbf{3}$ contains two irreducible representations, cf. Eq. (3.6), this basis must be complete. That means that the s-channel base tensors are linear combinations of these singlet structures. The projective prescription (3.7) leads to the following set of equations:

$$(A_I \delta_{ba_2}\delta_{b'a_1} + B_I \delta_{ba_1}\delta_{b'a_2})(A_{I'}\delta_{a_3 b'}\delta_{a_4 b} + B_{I'}\delta_{a_3 b}\delta_{a_4 b'}) = Z\delta_{II'}(A_I \delta_{a_3 a_2}\delta_{a_4 a_1} + B_I \delta_{a_3 a_1}\delta_{a_4 a_2}),$$

where $I, I' \in \{1, 2\}$ and Z is an arbitrary normalization constant. Working out the equations shows that up to interchanging the base tensors the unique solution is given by $A_1 = -A_2 = B_1 = B_2 = Z/2$, which is exactly the basis given in Eq. (3.9).

One can check explicitly that this basis is complete for gluon resummation: representing the combined colour structure of the external particles by one of the base tensors c_I and connecting any two external particles by an additional gluon yields no additional colour structures. In Fig. 9 an example of such a gluon insertion is shown. For processes for which the LO colour basis is not complete, this procedure can also be used to identify additional base tensors.

Figure 9: An example of gluon insertion.

If a particle is exchanged in the s-channel, the corresponding base tensor has a direct physical interpretation. An example is the Feynman diagram for the $qg \to \tilde{q}\tilde{g}$ process shown in Fig. 10. Since the quark exchanged in the s-channel is in the fundamental representation, the corresponding N_C-dimensional base tensor (c_1^{qg} in Eq. (3.11)) can be read off immediately from the colour structure of this diagram.
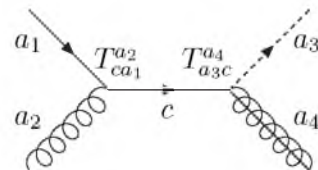

Figure 10: Example of a diagram corresponding to a base tensor.

C. Eikonal Feynman rules

In this appendix the eikonal Feynman rules will be given for a soft gluon with momentum k attached to an eikonal line with momentum p. In the eikonal approximation we have $k \ll p$, which leads to simple Feynman rules since the propagator that connects the matrix

element to the radiated gluon becomes effectively on-shell. The generic diagrams and their corresponding Feynman rules are given by (cf. [40])

$$= g_s(T_R^c)_{ab}\frac{p_\mu}{p \cdot k - i\epsilon} \tag{C.1}$$

for an incoming eikonal line and

$$= g_s(T_R^c)_{ab}\frac{p_\mu}{p \cdot k + i\epsilon} \tag{C.2}$$

for an outgoing eikonal line. Here g_s is the strong coupling constant, μ is the Lorentz index of the gluon and $i\epsilon$ represents the infinitesimal imaginary part of the propagator that connects the matrix element to the radiated gluon. The colour labels of the different particles are denoted by a, b and c. The representation of the eikonal line is denoted by R. We have $R = F$ for the fundamental representation, $R = \bar{F}$ for the charge conjugate of the fundamental representation, and $R = A$ for the adjoint representation. The colour operators occurring in Eqs. (C.1) and (C.2) are given in Table 3. Note that the order of the colour indices a, b, c in f_{abc} is kept fixed irrespective of whether the gluon is emitted above or below the eikonal line.

Outgoing (s)quark / incoming anti-(s)quark:	$(T_F^c)_{ab} = T_{ab}^c$
Outgoing anti-(s)quark / incoming (s)quark:	$(T_{\bar{F}}^c)_{ab} = -T_{ba}^c = -(T_{ab}^c)^*$
Gluons / gluinos:	$(T_A^c)_{ab} = F_{ab}^c = -if_{abc}$

Table 3: Colour operators used in the eikonal Feynman rules.

D. One-loop eikonal integral for $\tilde{\bar{q}}\tilde{g}$ production

We briefly present here the calculation of the kinematic part ω^{34} of the one-loop correction to the process $qg \to \tilde{\bar{q}}\tilde{g}$ in the eikonal approximation. The equal-mass case of ω^{34} is well known [40], but for $\tilde{\bar{q}}\tilde{g}$ final states we also need the unequal-mass version.

The kinematic part of the one-loop correction generated by the exchange of a virtual gluon between the two final-state eikonal lines is according to Eq. (C.2) given by

$$\omega^{34} = g_s^2 \int \frac{d^d k}{(2\pi)^d} \left(\frac{v_3}{v_3 \cdot k + i\epsilon} \right) \cdot \left(\frac{v_4}{-v_4 \cdot k + i\epsilon} \right) \frac{-i}{(k^2 + i\epsilon)} N^{\mu\nu}(k). \tag{D.1}$$

We use dimensionless vectors $v_i^\mu = p_i^\mu \sqrt{2/s}$ with p_i denoting the momentum of the massive external particle i. We calculate the gluon propagator in a general axial gauge with

$$N^{\mu\nu}(k) = g^{\mu\nu} - \frac{n^\mu k^\nu + k^\mu n^\nu}{n \cdot k} + n^2 \frac{k^\mu k^\nu}{(n \cdot k)^2}, \tag{D.2}$$

where n^μ is a general gauge vector with $n^2 < 0$. In the case that $v_{3,4}^2 > 0$ and $v_3^2 \neq v_4^2$ the solution of the integral ω^{34} reads

$$\omega^{34} = -\frac{\alpha_s}{\pi\epsilon} \left[L_{v_3,v_4} + L_{v_3} + L_{v_4} - 1 \right], \tag{D.3}$$

with $\epsilon = 4 - d$. The gauge-independent term L_{v_3,v_4} is given by

$$L_{v_3,v_4} = \frac{1}{2} \frac{v_3 \cdot v_4}{\sqrt{(v_3 \cdot v_4)^2 - v_3^2 v_4^2}} \left[2i\pi + \log\left(\frac{v_4^2 + v_3 \cdot v_4 - \sqrt{(v_3 \cdot v_4)^2 - v_3^2 v_4^2}}{v_4^2 + v_3 \cdot v_4 + \sqrt{(v_3 \cdot v_4)^2 - v_3^2 v_4^2}} \right) \right.$$
$$\left. + \log\left(\frac{v_3^2 + v_3 \cdot v_4 - \sqrt{(v_3 \cdot v_4)^2 - v_3^2 v_4^2}}{v_3^2 + v_3 \cdot v_4 + \sqrt{(v_3 \cdot v_4)^2 - v_3^2 v_4^2}} \right) \right]. \tag{D.4}$$

The gauge-dependent terms L_{v_3} and L_{v_4} can be found in Ref. [40] and cancel against contributions from the self-energy diagrams when calculating the anomalous dimensions. The gauge-independent term L_{v_3,v_4} can be rewritten in a compact form using β and κ as defined in Eqs. (2.2) and (3.4):

$$L_{v_3,v_4} = \frac{\kappa^2 + \beta^2}{2\kappa\beta} \left[\log\left(\frac{\kappa - \beta}{\kappa + \beta} \right) + i\pi \right]. \tag{D.5}$$

For equal-mass final-state particles this quantity reduces to the well-known form (cf. [27])

$$L_\beta = \frac{1 + \beta^2}{2\beta} \left[\log\left(\frac{1 - \beta}{1 + \beta} \right) + i\pi \right].$$

References

[1] Yu. A. Golfand and E. P. Likhtman, JETP Lett. **13**, 323 (1971) [Pisma Zh. Eksp. Teor. Fiz. **13**, 452 (1971)].

[2] J. Wess and B. Zumino, Nucl. Phys. B **70** (1974) 39.

[3] V. M. Abazov *et al.* [D0 Collaboration], Phys. Lett. B **660** (2008) 449 [arXiv:0712.3805 [hep-ex]].

[4] T. Aaltonen *et al.* [CDF Collaboration], Phys. Rev. Lett. **102** (2009) 121801 [arXiv:0811.2512 [hep-ex]].

[5] G. Aad *et al.* [The ATLAS Collaboration], arXiv:0901.0512 [hep-ex].

[6] G. L. Bayatian *et al.* [CMS Collaboration], J. Phys. G **34** (2007) 995.

[7] F. Gianotti, talk at the the 2009 Europhysics Conference on High Energy Physics, Krakow, Poland.

[8] H. P. Nilles, Phys. Rept. **110** (1984) 1.

[9] H. E. Haber and G. L. Kane, Phys. Rept. **117** (1985) 75.

[10] W. Beenakker, M. Krämer, T. Plehn, M. Spira and P. M. Zerwas, Nucl. Phys. B **515** (1998) 3 [arXiv:hep-ph/9710451].

[11] J. R. Ellis and S. Rudaz, Phys. Lett. B **128** (1983) 248.

[12] see e.g. H. Baer, V. Barger, G. Shaughnessy, H. Summy and L. t. Wang, Phys. Rev. D **75** (2007) 095010 [arXiv:hep-ph/0703289].

[13] G. L. Kane, A. A. Petrov, J. Shao and L. T. Wang, arXiv:0805.1397 [hep-ph].

[14] W. Beenakker, R. Höpker, M. Spira and P. M. Zerwas, Phys. Rev. Lett. **74** (1995) 2905 [arXiv:hep-ph/9412272].

[15] W. Beenakker, R. Höpker, M. Spira and P. M. Zerwas, Z. Phys. C **69** (1995) 163 [arXiv:hep-ph/9505416].

[16] W. Beenakker, R. Höpker, M. Spira and P. M. Zerwas, Nucl. Phys. B **492** (1997) 51 [arXiv:hep-ph/9610490].

[17] W. Hollik, M. Kollar and M. K. Trenkel, JHEP **0802** (2008) 018. [arXiv:0712.0287 [hep-ph]].

[18] W. Hollik and E. Mirabella, JHEP **0812** (2008) 087 [arXiv:0806.1433 [hep-ph]].

[19] W. Hollik, E. Mirabella and M. K. Trenkel, JHEP **0902** (2009) 002 [arXiv:0810.1044 [hep-ph]].

[20] E. Mirabella, arXiv:0908.3318 [hep-ph].

[21] A. T. Alan, K. Cankocak and D. A. Demir, Phys. Rev. D **75** (2007) 095002 [Erratum-ibid. D **76** (2007) 119903] [arXiv:hep-ph/0702289].

[22] S. Bornhauser, M. Drees, H. K. Dreiner and J. S. Kim, Phys. Rev. D **76** (2007) 095020 [arXiv:0709.2544 [hep-ph]].

[23] G. L. Kane and J. P. Leveille, Phys. Lett. B **112** (1982) 227.

[24] P. R. Harrison and C. H. Llewellyn Smith, Nucl. Phys. B **213** (1983) 223 [Erratum-ibid. B **223** (1983) 542].

[25] S. Dawson, E. Eichten and C. Quigg, Phys. Rev. D **31** (1985) 1581.

[26] A. Kulesza and L. Motyka, Phys. Rev. Lett. **102** (2009) 111802 [arXiv:0807.2405 [hep-ph]].

[27] A. Kulesza and L. Motyka, arXiv:0905.4749 [hep-ph].

[28] U. Langenfeld and S. O. Moch, arXiv:0901.0802 [hep-ph].

[29] M. Beneke, P. Falgari and C. Schwinn, arXiv:0907.1443 [hep-ph].

[30] M. Beneke, P. Falgari and C. Schwinn, arXiv:0909.3488 [hep-ph].

[31] K. Hagiwara and H. Yokoya, arXiv:0909.3204 [hep-ph].

[32] A. Idilbi, C. Kim and T. Mehen, Phys. Rev. D **79** (2009) 114016 [arXiv:0903.3668 [hep-ph]].

[33] G. Sterman, Nucl. Phys. B **281** (1987) 310.

[34] S. Catani and L. Trentadue, Nucl. Phys. B **327** (1989) 323.

[35] H. Contopanagos, E. Laenen and G. Sterman, Nucl. Phys. B **484** (1997) 303 [arXiv:hep-ph/9604313].

[36] N. Kidonakis, G. Oderda and G. Sterman, Nucl. Phys. B **525** (1998) 299 [arXiv:hep-ph/9801268].

[37] N. Kidonakis, G. Oderda and G. Sterman, Nucl. Phys. B **531** (1998) 365 [arXiv:hep-ph/9803241].

[38] R. Bonciani, S. Catani, M. L. Mangano and P. Nason, Nucl. Phys. B **529**, 424 (1998) [arXiv:hep-ph/9801375].

[39] J. Botts and G. Sterman, Nucl. Phys. B **325** (1989) 62.

[40] N. Kidonakis and G. Sterman, Nucl. Phys. B **505** (1997) 321 [arXiv:hep-ph/9705234].

[41] S. Catani, M. L. Mangano, P. Nason and L. Trentadue, Nucl. Phys. B **478** (1996) 273 [arXiv:hep-ph/9604351].

[42] A. Kulesza, G. Sterman and W. Vogelsang, Phys. Rev. D **66** (2002) 014011 [arXiv:hep-ph/0202251].

[43] A. D. Martin, W. J. Stirling, R. S. Thorne and G. Watt, Eur. Phys. J. C **63** (2009) 189 [arXiv:0901.0002 [hep-ph]].

[44] see http://www.thphys.uni-heidelberg.de/~plehn/prospino/ or http://people.web.psi.ch/spira/prospino/